Geoscience Frontiers xxx (2016) 1–17

HOSTED BY

ELSEVIER

Contents lists available at ScienceDirect

China University of Geosciences (Beijing)

Geoscience Frontiers

journal homepage: www.elsevier.com/locate/gsf

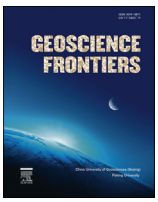

Research paper

Sedimentology, provenance and geochronology of the Miocene Qiuwu Formation: Implication for the uplift history of Southern Tibet

Jiawei Zhang, Jingen Dai*, Xinyu Qian, Yukui Ge, Chengshan Wang

State Key Laboratory of Biogeology and Environmental Geology, School of the Earth Science and Resources, China University of Geosciences, Beijing, 100083, China

ARTICLE INFO

Article history:
Received 5 February 2016
Received in revised form
12 May 2016
Accepted 21 May 2016
Available online xxx

Keywords:
Qiuwu formation
Provenance analysis
Dickinson diagram
Detrital zircon
Depositional environment

ABSTRACT

Located on the south of the Gangdese, the Qiuwu Formation has traditionally been considered as Eocene coal-bearing clastic sediments consisting of sandstone, mudstone and conglomerate, unconformably on top of Gangdese batholith. However, its precise age and depositional environment remain ambiguous. Here, we present a newly measured stratigraphic section near the Ngamring County, western Xigaze. Detrital zircon U–Pb ages were also applied to trace the provenance of sediments and to constrain the maximum depositional age of the Qiuwu Formation. Sedimentary facies analyses indicate subaqueous fan and alluvial fan depositional environments. Clast composition of the conglomerate is dominated by magmatic rocks at the lower part, while chert and mafic detritus occur in the upper part, suggesting a southern source. Sandstone modal analyses indicate that the compositions of quartz, feldspar and lithic grains changed from transitional arc to dissected arc, implying the unroofing of the Gangdese arc. Detrital zircon U–Pb ages of the Qiuwu Formation are compared with those from Gangdese magmatic rocks and Yarlung-Zangbo ophiolites, suggesting that the Gangdese arc is a main source of the Qiuwu detritus and that the southern source played a role during the later stage. The major peak of detrital zircon ages is at 45–55 Ma, which corresponds to Linzizong volcanic rocks in southern Gangdese arc. The weighted mean age of the five youngest zircons from the lower part of the section is 21.0 ± 2.2 Ma, suggesting that the Qiuwu Formation was deposited in early Miocene, coeval with other conglomerates exposed along the southern margin of Gangdese. Combining new observations with previously published data, we propose that the provenance of the Qiuwu Formation had shifted from a single northern source to double sources from both the north and the south. Activities of Great Counter Thrust were primarily responsible for the shift by making the south area a high elevation to provide sediments for the Qiuwu Formation.

1. Introduction

The Yarlung–Zangbo suture zone in the southern Tibetan Plateau not only preserves information of the Neo-Tethyan evolution, but also provides details of the India–Asia collision and the uplift history of the Tibetan Plateau and Himalayas (Aitchison et al., 2011; Wang et al., 2012; Dai et al., 2013a). In general, the Yarlung–Zangbo ophiolite, Xigaze forearc basin, and Gangdese magmatic arc (Fig. 1) are related to the evolution of Neo-Tethys and the India–Asia collision, while the late Cenozoic sedimentary basins within this suture zone provide a unique archive of uplift history.

The Liuqu and Kailas basins, both narrow and strike-parallel, are the most representative late Cenozoic sedimentary basins. The Liuqu basin is located in the south of the central Yarlung–Zangbo ophiolite, and is filled with Paleogene Liuqu conglomerate (Davis et al., 2002; Wang et al., 2010; Li et al., 2015a), containing abundant red chert cobbles, ultramafic–mafic cobbles, as well as quartz–arenite, litharenite, phyllite and slate. Davis et al. (2002) proposed that the Liuqu conglomerate probably formed during

* Corresponding author. Tel.: +86 10 82323678; fax: +86 10 82322171.
E-mail address: djgtibet@163.com (J. Dai).
Peer-review under responsibility of China University of Geosciences (Beijing).

http://dx.doi.org/10.1016/j.gsf.2016.05.010

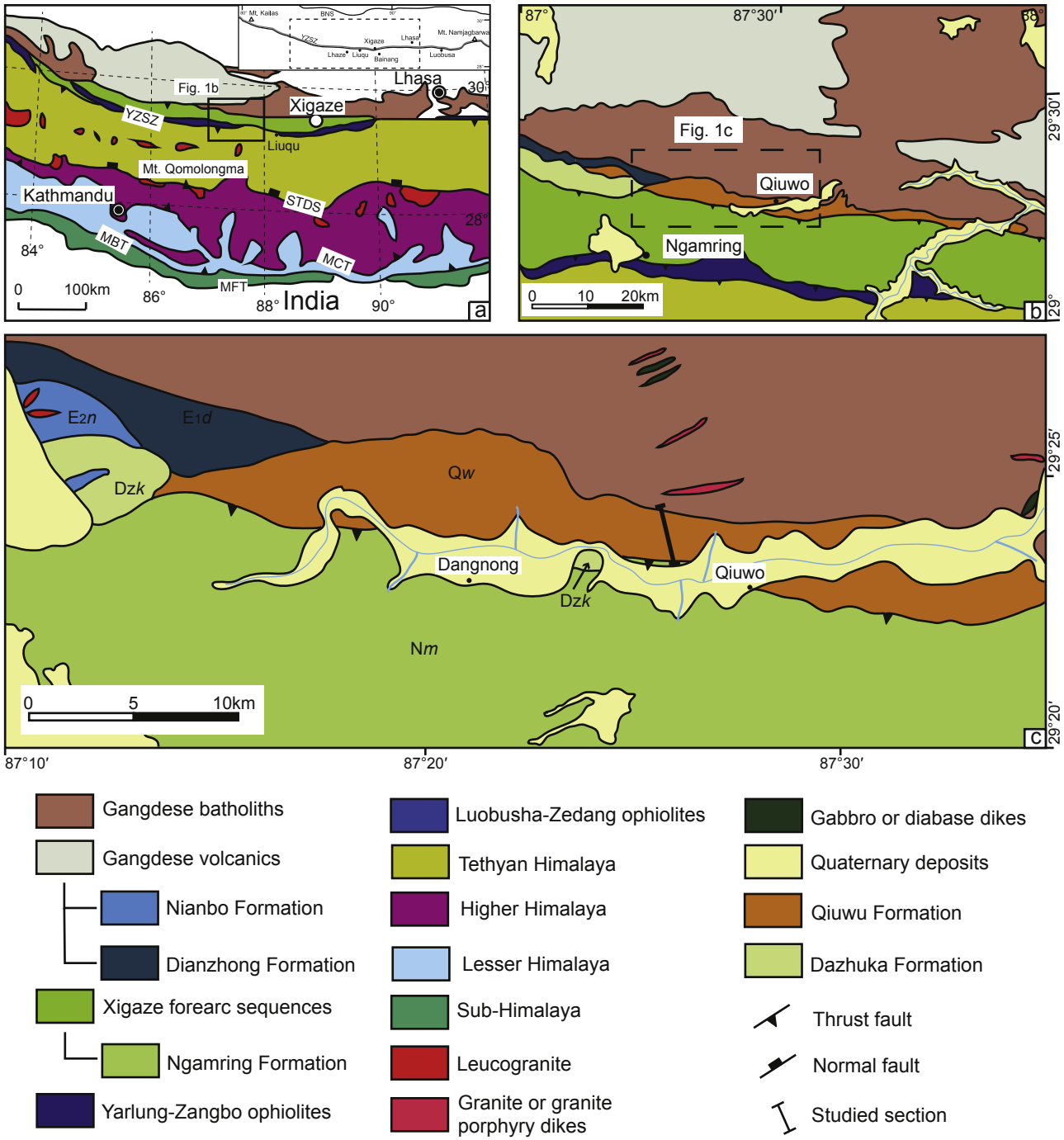

Figure 1. (a) Simplified geological map of the Himalaya and southern Tibet, modified after Wang et al. (2013). BNS = Bangong-Nujing suturse; YZSZ = Yarlung-Zangbo suture zone; STDZ = South Tibet Detachment Zone; MCT = Main Central Thrust; MBT = Main Boundary Thrust; MFT = Main Frontal Thrust. (b) Geological sketch map of the Ngamring area, southern Tibet, modified after a scale of 1:1,500,000 geologic map (Pan et al., 2004). (c) Detailed geological map of the studied area, modified after a scale of 1:250,000 geologic map resulted from regional geological survey, showing location of measured sections (black bold segment). E_2n = Nianbo Formation; E_1d = Dianzhong Formation; Qw = Qiuwu Formation; Dzk = Dazhuka Formation; Nm = Ngamring Formation.

the collision between an intra-oceanic arc and the Indian continental margin. However, subsequent studies indicate that the Liuqu conglomerate contains clasts originated from both the Langjiexue Group and Tethyan Himalayan sediments to its south, as well as the sediments within the Xigaze forearc basin and the ophiolite to its north (Wang et al., 2010; Li et al., 2015a). Particularly, Li et al. (2015a) suggested that the Liuqu conglomerate preserved the post-collision erosion in the Indus–Yarlung suture zone. The Kailas basin is characterized by the Kailas conglomerate (Aitchison et al., 2002; DeCelles et al., 2011), which crops out along the entire Yarlung–Zangbo suture zone, stretching from the Kailas Mountain in the west to Namjagbarwa Mountain in the east. The Kailas conglomerate is referred to different stratigraphic names in different areas, such as Kailas, Qiuwu, Dazhuka and Luobusa

Please cite this article in press as: Zhang, J., et al., Sedimentology, provenance and geochronology of the Miocene Qiuwu Formation: Implication for the uplift history of Southern Tibet, Geoscience Frontiers (2016), http://dx.doi.org/10.1016/j.gsf.2016.05.010

formations (Gansser, 1964; Badengzhu, 1979, 1981; Zhang and Fu, 1982; Wei and Peng, 1984). Based on the geochronology and sedimentology of the Kailas Formation in the west, DeCelles et al. (2011) proposed that the Kailas Formation was deposited during late Oligocene to early Miocene time, and was formed in alluvial fan, low-sinuosity fluvial, and deep lacustrine depositional systems. Wang et al. (2013) investigated the age and depositional environment of the Qiuwu and Dazhuka formations—the geographically central part of Kailas conglomerate—and showed that the source areas of the Dazhuka Formation (braided-river deposits, 23–18 Ma) were the Gangdese arc and the Himalayan orogen. The underlying Qiuwu Formation was deposited in lacustrine and deltaic environments during latest Oligocene to earliest Miocene (ca. 23 Ma) with an exclusive provenance from the Gangdese magmatic arc north to Qiuwu Formation. However, the Qiabulin section studied by Wang et al. (2013) might not contain the complete Qiuwu Formation, especially the upper part.

In order to test whether the whole Kailas basin was formed simultaneously in similar depositional settings, and to track the provenance of the Qiuwu Formation, we measured the Qiuwu section in central part and present detailed data of petrology, stratigraphy, sedimentology and U–Pb ages of detrital zircons in sandstones. Our study reveals that the Qiuwu Formation was formed in subaqueous fans and alluvial fans during early Miocene and consists of sediments from both the north and the south.

2. Geological setting

The Tibetan Plateau consists of several blocks, including Himalayas, Lhasa, Qiangtang and Songpan–Ganze, divided by several near east-west trending suture zones (Yin and Harrison, 2000; Dai et al., 2011). The Yarlung–Zangbo suture zone (YZSZ) lies in the southernmost plateau (Fig. 1a), and consists of several tectonic-sedimentary units, including Qiuwu Formation, Dazhuka Formation, Xigaze forearc basin, Yarlung–Zangbo ophiolite, Liuqu Formation and mélange. These units preserve detailed information of Neo-Tethys, the India–Asia collision and subsequent plateau uplift.

The Gangdese arc is the southernmost part of the Lhasa block, adjacent to the YZSZ. Composed of Mesozoic–early Paleogene granitoids, and Paleogene terrestrial volcanic rocks (Fig. 1a; Mo et al., 2008; Chu et al., 2011), the Gangdese arc experienced several stages of exhumation, including Cretaceous–early Paleogene, Eocene (46–48 Ma), early Miocene (22–18 Ma) and middle Miocene (11–8 Ma) (Dai et al., 2013a). The Qiuwu Formation crops out along the YZSZ, displaying a narrow belt between the Gangdese arc and the Xigaze forearc basin (Fig. 1b). Being a set of coal-bearing clastic sediments, Qiuwu Formation is composed of sandstones and mudstones interbedded with conglomerates (Yin et al., 1988; Li et al., 2008). The main component of Dazhuka Formation is conglomerates with the clast composition of ultra-mafic and mafic rocks and radiolarian cherts (Aitchison and Davis, 2002; Li et al., 2010; Wang et al., 2013). The Xigaze forearc basin is dominated by Cretaceous flysch sediments known as Ngamring Formation (Fig. 1b, c), which recorded early exhumation of the Gangdese arc (Einsele et al., 1994; Dürr, 1996; Wu et al., 2010; Wang et al., 2012; Dai et al., 2013b; An et al., 2014; Orme et al., 2015). The Yarlung–Zangbo ophiolite comprises mantle peridotite, grabbo, diabase dike, sheeted sill, basalt and abyssal sediments containing radiolarian chert (Dai et al., 2012, 2013b). Liuqu Formation crops out in a limited area of ca. 150 km between Lhaze and Bainang (Li et al., 2015a). The mélange is a narrow, elongated belt, which located in the accretionary wedge. South of the YZSZ, the Himalayas consists of four major geologic domains (Fig. 1a) (Yin, 2006). Adjacent to the YZSZ, the Tethyan Himalaya was separated from the High Himalaya at the south part by the South Tibetan Detachment System. The Tethyan Himalaya consists of Proterozoic to Eocene siliciclastic and carbonate rocks interbedded with Paleozoic and Mesozoic volcanic rocks (Yin, 2006).

3. Stratigraphy and sedimentology

We measured an 840-meter-thick section of the Qiuwu Formation in northeastern Ngamring, Xigaze, Tibet. The GPS location of the section is 29°22′39″N, 87°25′39″E.

3.1. Stratigraphy

Qiuwu Formation is deposited on the underlying Gangdese magmatic rocks in the north, and in fault contact (see the panorama and contact between two stratums in Supplementary Fig. S1) with the overlying Ngamring Formation flysh sediments in the south. Based on the lithofacies assemblage, the measured section of the Qiuwu Formation can be divided into three parts.

The lower part is approximately 383 m in thickness and gray or dark gray in color (Fig. 2a), characterized by matrix- and clast-supported conglomerate (Gmm, Gcm), coarse- to medium-grained massive sandstone (Sm), massive and laminated siltstone (Fsm, Fl) and shale. Coal seam (C) and plant fossils are present in several beds. The bottom of this part is gray clast- and matrix-supported conglomerate whose clasts mainly consist of disorganized granite and occasionally andesite. The gravels are mainly angular or subangular (Fig. 2b) cobbles or boulders. Normal grading structure (Gmg) has been observed. The sediments fine up into grayish–green massive argillaceous lithic sandstone with stratified marl nodules (Fig. 2c) and pisolitic pyrite (Fig. 3b). Individual sandstone bed is 5–20 cm thick. The uppermost of this part is gray and dark gray coal-bearing shale (Fig. 2e) and lenticular sandstone (Sl) with marl nodules and plant fossil fragments (Fig. 2f). Most sandstones beds only stretch for tens of meters laterally.

The middle part of the studied section is 303 m thick, defined by red, clast-supported, moderately to poorly sorted conglomerate (Gcm), grayish-green medium- to fine-grained massive or plane-parallel laminated sandstones (Sm, Sh), red moderately well-sorted argillaceous sandstones (Fig. 2d), massive and laminated siltstones (Fsm, Fl) and massive mudstones (Fm). The dominated lithofacies is Gcm, and its size gradually transitioned into cobble and pebble. Sandstones are interbedded with shales or mudstones (Fig. 2d), and lenticular conglomerates, while some of the sandstone beds also contain granitic pebbles. Individual sandstone bed at the bottom is usually 5–10 cm thick, but they become thicker to 80 cm at the top. Sedimentary structures are rare and plant fossils are absent.

The upper part is 158 m in thickness, and consists of red, very fine- to medium-grained, massive or plane-parallel laminated argillaceous sandstone and lithic sandstone (Sm, Sh), sandstone with cross bedding (Sp), massive and laminated siltstone (Fsm, Fl), shale and massive mudstone (Fm), and conglomerate (Fig. 2g). Parts of sandstones and mudstones bear pebbles or cobbles. Erosional bases are observed in the coarse-grained sandstone beds, which are about 5–10 cm thick. A clast-supported lenticular conglomerate appears at the top, which is well-sorted and consists of sub-rounded to rounded granites, abundant cherts and mafic (Fig. 6h) gravels that are 2–5 cm in size. The conglomerate lense is a few meters in width.

3.2. Sedimentology

Based on lithology, sedimentary structure, and observation of thin sections, the Qiuwu Formation can be divided into the following lithofacies: conglomerate facies, sandstone facies, siltstone facies and mudstone facies (Fig. 4, Table 1 and references therein).

Please cite this article in press as: Zhang, J., et al., Sedimentology, provenance and geochronology of the Miocene Qiuwu Formation: Implication for the uplift history of Southern Tibet, Geoscience Frontiers (2016), http://dx.doi.org/10.1016/j.gsf.2016.05.010

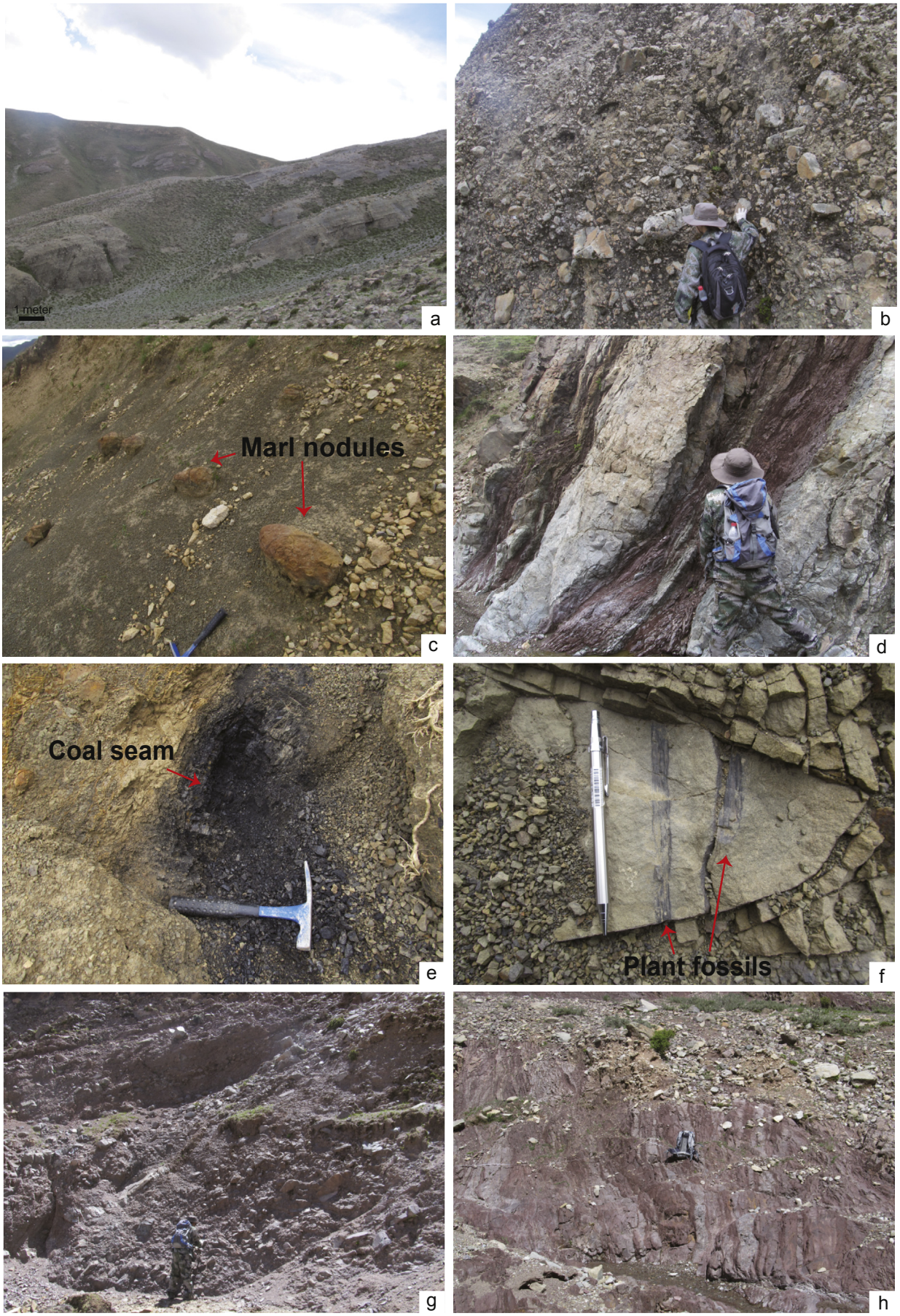

Please cite this article in press as: Zhang, J., et al., Sedimentology, provenance and geochronology of the Miocene Qiuwu Formation: Implication for the uplift history of Southern Tibet, Geoscience Frontiers (2016), http://dx.doi.org/10.1016/j.gsf.2016.05.010

Figure 3. Photographs of sedimentary structures in the Qiuwu section. (a) Normal grading structure in granitic gravels at the bottom. The gravels are angular to subangular. Hammer is 35 cm long. (b) Pisolitic pyrite preserved in lithic sandstones. Many joints cut across sandstone beds. The pyrites are centimeter in size. Hammer is 35 cm long. (c) Groove cast formed of gravity. The sandstones are very strongly weathered. Pencil is 10 cm long. (d) Erosional surface between sandstones and siltstones. The stratum is strongly deformed. Hammer is 35 cm long. (e) Fining-upward sedimentary cycles reflecting the pulse of water. Five cycles in this area of outcrop could be observed. Hammer is 35 cm long. (f) Cross bedding indicating paleocurrent direction. Marker pen is 9 cm long. The orientation of each photo is marked at the upper right.

3.2.1. Lithofacies

3.2.1.1. Conglomerate facies (Gcm, Gmm and Gmg). The conglomerate facies widely appear through the section. The facies are characterized by a set of 130-meter-thick, poorly sorted angular or subangular gray conglomerates (Fig. 2a, b), lying unconformably upon the Gangdese granites. The average grain sizes are tens of centimeters, but a few particularly large clasts are over 2 m in long dimension. Clast composition is large granites and a few andesites.

Figure 2. Field photographs of Qiuwu Formation outcrops. (a) Stratified conglomerate at the bottom of Qiuwu Formation. Although it is not well outcropped in some place, the beds are obvious to observe. (b) Poorly sorted and organized granitic gravels. At the bottom of the section, the compositions of gravels are granite with no indicative structure. Person is 1.7 m tall. (c) Marl nodules in the mudstone. The mudstone is strongly weathered. Marl nodules are bulgy due to differential weathering. Hammer is 35 cm long. (d) Thick-bedded sandstone interbedded with red shale in the middle of the section. Sandstone beds are 1.2 m thick and shale beds are much thinner. Person is 1.7 m tall. (e) Coal seam buried in the yellow mudstone. Hammer is 35 cm long. (f) Plant remnants preserved in the siltstone, which could not be classified into specific species. Pencil is 12 cm long. (g) Red conglomerate beds deposited in the upper part of the section. The gravels are much smaller and more complicated than those at the bottom (see Fig. 6). Person is 1.7 m tall. (h) Fine sandstone beds. Some beds are interbedded with lenticular conglomerate. Schoolbag is 60 cm long. The orientation is marked at the upper right of each photo.

Please cite this article in press as: Zhang, J., et al., Sedimentology, provenance and geochronology of the Miocene Qiuwu Formation: Implication for the uplift history of Southern Tibet, Geoscience Frontiers (2016), http://dx.doi.org/10.1016/j.gsf.2016.05.010

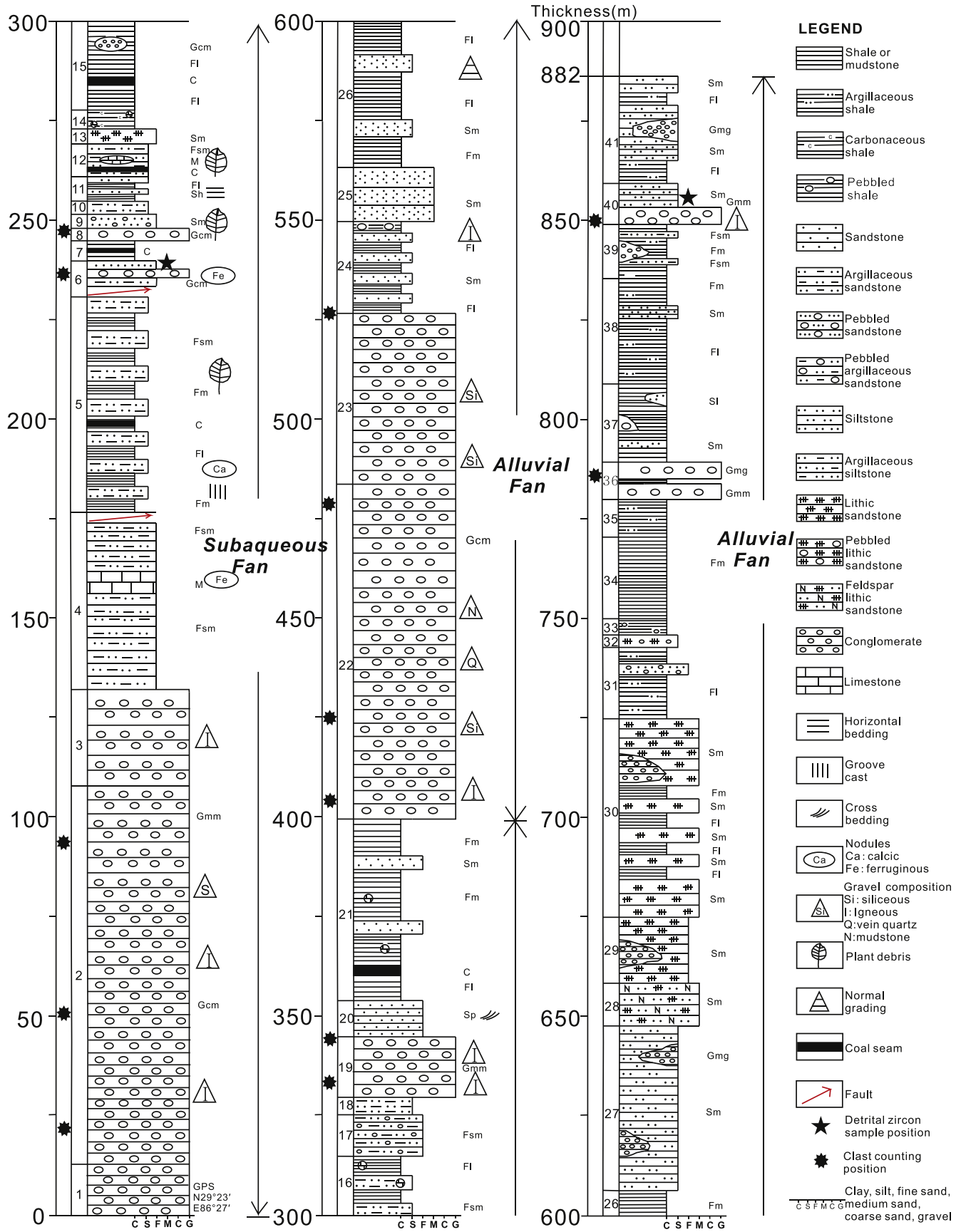

Figure 4. Log of Qiuwu section, signed with lithofacies, sedimentary structures, depositional environment, clast counting positions and sandstone sample locations for detrital zircon analyses. See Table 1 for lithofacies code.

Please cite this article in press as: Zhang, J., et al., Sedimentology, provenance and geochronology of the Miocene Qiuwu Formation: Implication for the uplift history of Southern Tibet, Geoscience Frontiers (2016), http://dx.doi.org/10.1016/j.gsf.2016.05.010

Table 1
Description of lithofacies and interpretation of the Qiuwu Formation (after Miall, 1996).

Facies code	Description	Process interpretation
Gcm	Pebble to cobble conglomerate, poorly sorted, clast-supported, massive, poorly organized	Sheedfloods or clast-rich debris flows
Gmm	Pebble to cobble conglomerate, poorly sorted, matrix-supported, massive, disorganized	Deposition of cohesive mud-matrix debris flows
Gmg	Pebble to cobble conglomerate, moderately sorted, matrix-supported, normal grading	Deposition by debris flows or braided river channel deposits
Sm	Massive coarse-to fine-grained sandstone, sometimes pebble, differ in layer thickness	Gravity flow deposits in alluvial fan or overbank setting
Sl	Fine-to medium-grained sandstone, moderately sorted, lenticular	Deposition by alluvial fan or delta bar
Sp	Medium-to coarse-grained sandstone with planar cross stratification	Migration of 2-D ripples under moderately powerful unidirectional channelized flows or migration of sandy transverse bars
Sh	Very fine-to medium-grained sandstone with plane-parallel lamination	Upper plane bed conditions under strong, either unidirectional flows or very shallow
Fl	Siltstone or mudstone with horizontal lamination, containing plant fossil parts	Deposition of abandoned channel, distal fan or floodplain
Fsm	Massive siltstone, usually red	Deposition by floodplain or abandoned channel
Fm	Massive mudstone	Floodplain, lake, backswamp or distal fan
M	Micritic massive gray and yellow marl	Lacustrine carbonate mud deposits
C	Coal or carbonaceous mud	Deposition of distributary bay or plant-rich swamp

Chert and mafic detritus occur in the upper part of the section. The matrix is mainly argillaceous. Most conglomerates are clast-supported, with matrix-supported mainly exposed in the lower unit. The conglomerate was probably deposited in mud-matrix debris flows on an alluvial fan (Blair and McPherson, 1994).

3.2.1.2. Sandstone facies (Sm, Sl, Sp and Sh). The sandstone facies crop out in the middle and upper part of the section. Main components of the facies are yellow-gray lithic quartz sandstone, litharenite, arkose and pebbled sandstone. Pyrite nodules are present in some sandstone beds. The grains in sandstones are moderately sorted, with subrounded to subangular appearance. The modal percent of quartz is 55–90%, while feldspar varies from 10% to 35%. The volcanic detritus are mainly argillaceously cemented. Fining-upward cycles (Fig. 3e) are observed, suggesting pulses of water flow. Most sandstones are massive and plane-parallel laminated. Cross beddings are preserved in the upper beds (Fig. 3f), and some coarse-grained sandstone beds develop erosional bases. Sandstone beds are usually 5–20 cm thick. These facies are attributed to subaqueous deposition of a fan delta (Weirich, 1988; Horton and Schmitt, 1996) or an alluvial fan (Smith, 1986; Blair and McPherson, 1994).

3.2.1.3. Siltstone facies (Fsm, Fl). The siltstone facies are observed in the middle and at the top of the section. The siltstones are characterized by its grayish-yellow color and argillaceously cemented texture, while its mineral composition is identical with that of sandstones. Individual siltstone bed is typically 5–10 cm thick, and some beds contain erosional surface on the top (Fig. 3d). The majority of siltstone beds are massive or with plane-parallel lamination. It is suggested that such facies may indicate deposition of abandoned channels or a distal fan (Miall, 1977; Blair and McPherson, 1994).

3.2.1.4. Mudstone facies (Fm). The massive coal-bearing gray or ash black mudstone (Fig. 2e) is interbedded with stratified synsedimentary globosity limestone. The mudstones typically appear as thin layers with lamination, which could be interpreted as suspension deposits in lacustrine depositional environments (Link and Osborne, 1978).

3.2.2. Depositional environment

The Qiuwu Formation was deposited in two distinctive stages, characterized by different depositional environment. The early stage is represented by an up-fining sequence at the bottom of the section. The conglomerate is mostly disorganized, containing poorly sorted and angular-sub-angular granitic gravels and few andesitic gravels. The normal grading (Fig. 3a), matrix- and clast-supported conglomerate (Gmg, Gmm, Gcm) represents root fan. Marl-bearing (Fig. 2c) and pyrite nodules-bearing (Fig. 3b) sandstones (Sm) and sandstones containing groove cast (Fig. 3c) on basal face represent inner–middle fan. Siltstones (Fl, Fsm), coal beds (C) and shales represent rim fan. The lithology is characterized by high proportion of poorly sorted coarse fragments, indicating that the detritus was deposited close to the source. These deposits are representative of debris flows on both subaerial and subaqueous parts of a fan delta (lacustrine fan delta) (Horton and Schmitt, 1996). Very fine debris or clay was found in the matrix of conglomerate, which makes large gravels appear to be suspending (Fig. 2b). This indicates the deposition of subaqueous debris flow (Walker, 1978). With a maturity index (Q/F + L) of ca. 0.3, the compositional maturity of sandstone is very low, which is a significant feature of subaqueous fan (Pettijohn, 1957). Graded bedding and massive structure are observed. Plant fossils are preserved, indicating that they were formed in a weakly oxic or a reducing environment, which result in gray, green, brown or black sediments. As a conclusion, we infer that the lower part of the section, featuring facies Gmg, Gmm, Gcm, Sm Fl, Fsm, M and C, was deposited in a subaqueous fan (Yu et al., 2006; Olivier et al., 2012). The grayish color of sediments and the presence of terrestrial plant fossils further indicate a lacustrine fan deposition, rather than a marine environment. The conclusion is consistent with previous studies that Neo-Tethys had disappeared since late Eocene (Searle et al., 1987; Wang et al., 2002; Ding et al., 2005; Aitchison et al., 2007).

The upper part of the section is also an up-fining sequence, but demonstrates more variable lithological features. The color shows darker shade in purple (Figs. 2g and 3d, f) than the lower section, which indicates an oxidation environment. Conglomerates (Gcm) have sand, silt and clay filling the vacancies between pebbles and cobbles, which is attributed to deposition of poorly developed

Please cite this article in press as: Zhang, J., et al., Sedimentology, provenance and geochronology of the Miocene Qiuwu Formation: Implication for the uplift history of Southern Tibet, Geoscience Frontiers (2016), http://dx.doi.org/10.1016/j.gsf.2016.05.010

gravel bars on a proximal alluvial fan (Nemec and Postma, 1993; Ridgway and DeCelles, 1993; Horton et al., 2002). Compositional and structural maturity of the sediments are still very low, suggesting a short-distance transport. The above features suggest deposition in erosive, turbulent water flows of high competence rather than in laminar debris flows (Horton et al., 2002). Erosional surface (Fig. 3d) and fining-upward cycles (Fig. 3e), preserved in the sandstones, also suggest a high-energy water flow (Gillet et al., 2007). In conclusion, the upper part of the section, featuring facies Gcm, Sm, Sp, Sh, Fsm and Fm, indicates an alluvial fan environment.

4. Provenance analysis: samples and methods

Provenance analysis was mainly conducted by using conglomerate clast counts, paleocurrent, sandstone modal compositions and detrital zircon U–Pb ages. Over 1000 gravels were counted in the field. A total of 54 thin sections were observed, among which 22 were counted using the Gazzi–Dickinson method (Ingersoll et al., 1984). Two sandstones from the bottom (QW12-06U1) and the top (QW12-40U1), respectively, were separated for detrital zircon analyses.

4.1. Conglomerate clast counts

Conglomerate composition was determined and recorded in the field by counting clasts on different conglomerate outcrops within a 1 m^2 grid. Occasionally, the grid was moved laterally, but still on the same bed, to manage a minimum count of 100 clasts each position (Orme et al., 2015). In some cases, the clasts were counted less than 100 because of bad exposure. In total, 1229 clasts were counted at 13 locations (Table 2).

4.2. Paleocurrent

Paleocurrents information were predominantly obtained from imbricate structures within conglomerate beds at six locations and from one cross bedding developed in sandstone. About 120 paleocurrent indicators indicate dispersal patterns along the section. All paleocurrent data were corrected with horizontal bedding rotations using Stereonet 8 (Allmendinger et al., 2012).

4.3. Modal sandstone petrology

Petrographic analyses were performed using the Gazzi–Dickinson method, with at least 300 points counted for each sample (Ingersoll et al., 1984). Triangular diagrams showing framework proportions of different grain sources could successfully distinguish the main provenance types (Dickinson and Suczek, 1979). Dickinson and Suczek (1979) and Dickinson (1985) have classified all provenances into three general groups and several variants, establishing four complementary models, Qt–F–L, Qm–F–Lt, Qp–Lv–Ls and Qm–P–K (the abbreviations are elaborated in the next part). The tectonic setting interpretation and provenance analysis can be carried out by choosing specific model or combining them.

Statistical analysis of thin sections under microscope should be carried out before the result is plotted into triangular diagrams. Since the numerical ratio of grains approximately equals to the area ratio (Dickinson, 1985; Chu and Li, 2007), the easy-to-operate point-counting method is adopted in this study. In practice, the average size of grains should be > 0.0625 mm and <2 mm. For each sample, we counted ca. 300 particles of each kind, including monocrystalline quartz (Qm), polycrystalline quartzose lithic fragments (Qp), plagioclase (P), potassium feldspar (K), sedimentary lithic fragments (Ls), metamorphic lithic fragments (Lm) and volcanic lithic fragments (Lv), respectively.

4.4. Detrital zircon geochronology

Two sandstone samples from the bottom (QW12-06U1) and the top (QW12-40U1), respectively, of the section (Fig. 4) were analyzed. Zircon concentrates were separated from the samples using standard density and magnetic separation techniques. Each individual crystal was handpicked and mounted in epoxy resin along with standard zircon. Zircon U–Pb dating was performed by laser ablation inductively coupled plasma-mass spectrometry (LA-ICP-MS) at the State Key Laboratory of Mineral Deposit Research, Nanjing University, China.

Element and isotope ion–signal intensities were acquired by Agilent 7500a ICP-MS instrument. Australian standard zircon (Jackson et al., 2004) was used to calibrate U–Pb dating. Standard zircon Mud Tank (Black and Gulson, 1978) was analyzed as internal standard for controlling accuracy. For details of the instrumental conditions and processes of data acquisition, see Griffin et al. (2004) and Jackson et al. (2004). Common Pb correction and ages of sample were calibrated and calculated using ComPbCorr#3–151 (Andersen, 2002). U–Pb weighted mean age calculations and probability density plots of U–Pb ages were made using Isoplot (Ludwig, 2001). Zircon U–Pb ages are given in Supplementary Table S1. Analyses were filtered with a 10% precision cutoff. In this study, $^{207}Pb/^{206}Pb$ ages are used to construct the age histograms for a few zircons older than 1000 Ma. $^{206}Pb/^{238}U$ ages are used for zircons younger than 1000 Ma, because the relatively small

Table 2
Clast counting results for the conglomerates from the Qiuwu Formation.

Position (m)[a]	23	51	95	228	249	331	340	403	425	477	527	781	850
Granite	72	69	50	16	18	18	20	0	0	21	2	1	4
Andesite	21	20	32	26	20	42	32	42	26	1	0	13	38
Dacite	8	5	10	47	12	12	2	0	0	0	0	0	0
Diorite	0	2	6	9	9	6	26	0	0	0	0	0	0
Granodiorite	0	1	1	0	6	2	2	0	0	0	0	0	0
Sandstone	0	0	0	1	1	0	0	0	2	0	0	0	0
Silicite	0	0	0	0	0	0	0	40	60	20	36	34	44
Diabase	0	0	0	0	0	0	0	8	20	10	9	17	15
Basalt	0	0	0	0	0	0	0	3	5	3	8	4	11
Vein quartz	0	0	0	1	0	6	0	10	20	13	16	8	12
Conglomerate	0	0	0	0	0	0	0	0	1	1	0	0	0
Mud	0	0	0	0	0	0	0	0	5	1	4	0	2
Other	0	0	0	0	0	0	0	0	0	2	2	0	4
Total	101	97	99	100	66	86	82	103	139	72	77	77	130

[a] Position indicates the stratigraphic level in Figs. 4 and 5.

Please cite this article in press as: Zhang, J., et al., Sedimentology, provenance and geochronology of the Miocene Qiuwu Formation: Implication for the uplift history of Southern Tibet, Geoscience Frontiers (2016), http://dx.doi.org/10.1016/j.gsf.2016.05.010

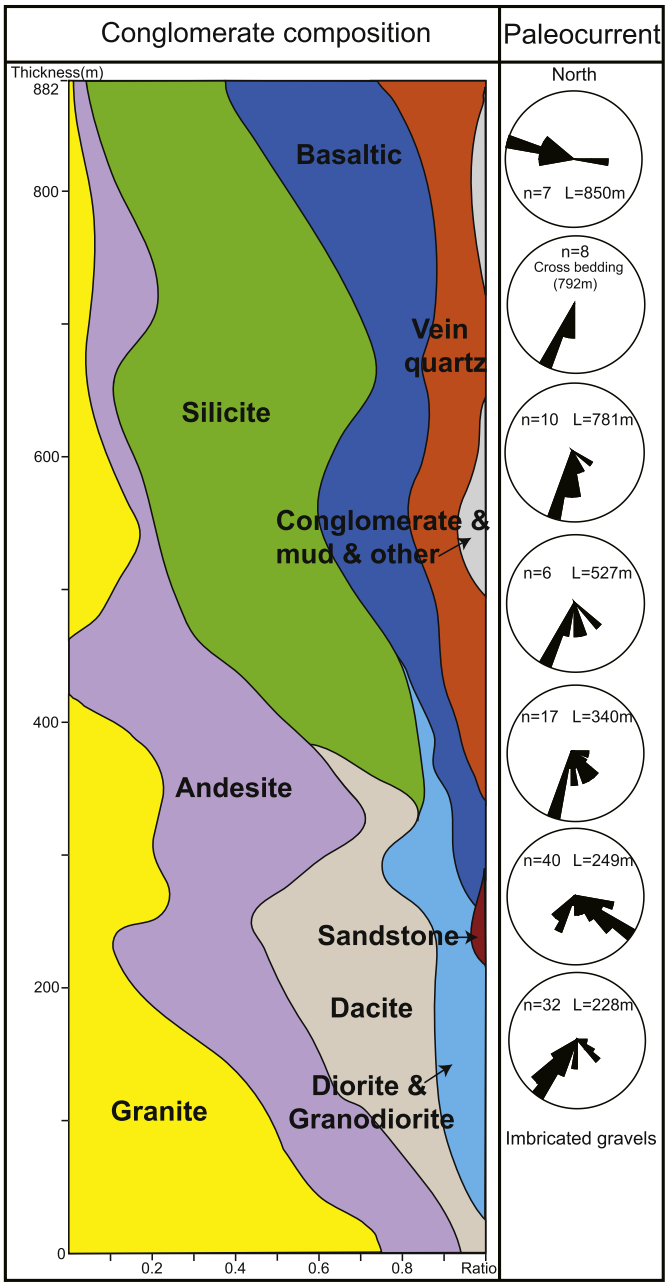

Figure 5. Clast count and paleocurrent results for Qiuwu Formation. Clast composition data are shown in Table 2. Paleocurrent data were measured from imbricate structures within conglomerate beds and one was from cross bedding within sandstone. The thickness of the column is consistent with Fig. 4. The solid circles in the left column represent counting positions.

amount of ^{207}Pb accumulated in young zircons does not permit precise $^{207}Pb/^{206}Pb$ dating (Griffin et al., 2004).

5. Provenance analysis: results

5.1. Conglomerate clast counts

The lower part of the Qiuwu Formation is dominated by granitoid, volcanic and hypabyssal clasts, with a small amount of sandstones, vein quartz and no chert (Fig. 5). The composition of gravels in the lower part is relatively simple. With most gravels igneous (Fig. 6a–c), the detailed proportions are as follows: granite, 20–70%; andesite, 10–50%; dacite, 8–40%; diorite and granodiorite, 0–20%; sandstone, 0–1%. The upper part, however, contains numerous chert and mafic (diabase, basalt) gravels (Fig. 6d–h), with a small amount of reworked conglomerates, granites, volcanics and sandstone clasts (Fig. 5). Compared with the lower part, the percentage of igneous clasts, mostly granite and andesite, decreases to 5–25%, the percentage of red and green cherts increases to 30–60%, and diabase and basalt increases to 10–20%. Vein quartz clasts firstly appear with cherts and its proportion remains stable at 5–10%. In the upper part, the composition of gravels becomes complicated, with conglomerate, mud and other clasts accounting for 1–2%.

5.2. Paleocurrent

Paleocurrent data indicate that sediments were mainly transported toward the south (Fig. 5), suggesting that they originated from the north area. In the upmost part, a westward paleoflow was observed (Fig. 5).

5.3. Modal sandstone petrology

The statistic results are shown in Table 3 and the microscope photos are shown in Fig. 7. Litharenites from the lower part of the Qiuwu Formation are volcaniclastic (Fig. 7), with a composition of Qt:F:L = 31:36:33 and Qm:F:Lt = 25:36:39, and they plot in the transitional and dissected magmatic-arc provenance fields of Dickinson (1985) (Fig. 8a). Quartz grains are angular to subangular and mostly monocrystalline with uniform extinction. Feldspar consists mainly of plagioclase, and volcanic lithic fragments are mostly felsic in composition.

Sandstones within the upper part of the Qiuwu Formation have average modal compositions of Qt:F:L = 47:28:25 and Qm:F:Lt = 42:28:30, and they plot in the dissected arc and recycled orogen provenance fields (Fig. 8a). Angular to subangular monocrystalline quartz is the primary component of total quartz grains within the samples. The proportion of quartz grains increases. Ultramafic detritus was barely observed in lithic fragments.

On the QFL ternary diagram (Fig. 8a), the lower part of the Qiuwu Formation concentrates in magmatic arc provenance. In contrast, the upper part presents the dissected arc provenance, with a large number of data points occupying the recycled orogen provenance. Though the span is large, there is a concentrated area and the plots show a progressive change, suggesting upward-increasing contributions from plutonic rocks and the possible recycling of old orogen rocks (Fig. 8b).

The Qp–Lv–Ls ternary diagram is especially helpful to discriminate magmatic arc suites from other groups (Dickinson and Suczek, 1979). The Qiuwu Formation was mainly derived from magmatic arc provenance as stated above. On the Qm–P–K diagram, the sandstones fall in a broad arcuate field, suggesting an increase in maturity or stability, probably attributing to the more detritus provided by collision orogens and continental blocks. To summarize, sediments of the Qiuwu Formation were mainly derived from nearby magmatic arc, and the Yarlung–Zangbo accretionary wedge or Xigaze forearc basin.

5.4. Detrital zircon geochronology

A total of 180 zircon grains were collected from two sandstone samples for U–Pb age dating (Supplementary Table S1). Detrital zircon U–Pb ages of sandstone from the bottom (QW12-06U1)

Please cite this article in press as: Zhang, J., et al., Sedimentology, provenance and geochronology of the Miocene Qiuwu Formation: Implication for the uplift history of Southern Tibet, Geoscience Frontiers (2016), http://dx.doi.org/10.1016/j.gsf.2016.05.010

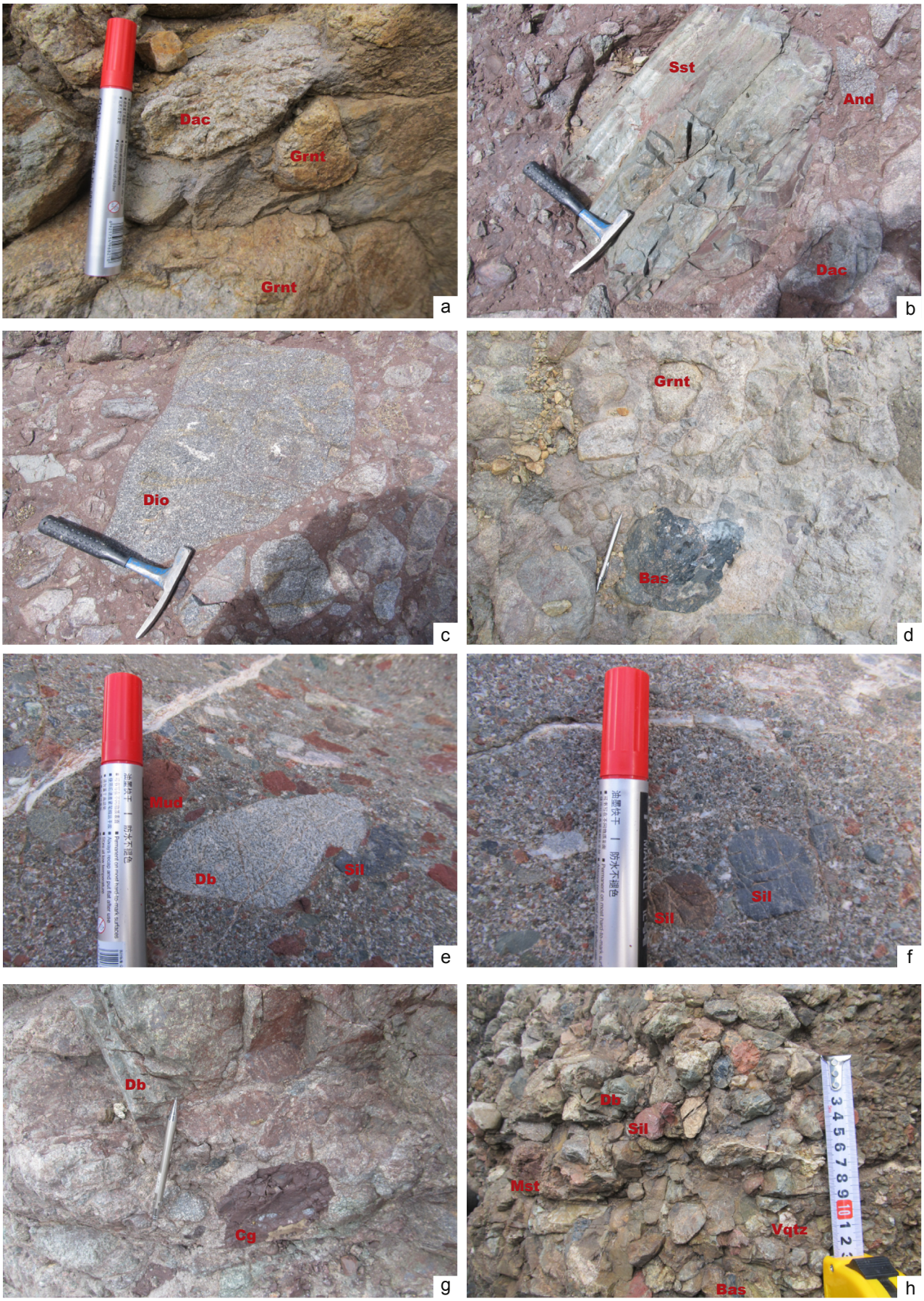

Figure 6. Representative clasts in Qiuwu Formation. Abbreviations: And = andesite; Bas = basalt; Cg = conglomerate; Dac = dacite; Db = diabase; Dio = diorite; Grnt = granite; Mst = mudstone; Ch = chert; Sst = sandstone; Vqtz = vein quartz. The scale in photographs: mark pen is 9 cm long; hammer is 35 cm; pencil is 12 cm; the exposure of steel tape is 13 cm. The orientation of each photo is marked at the upper right.

Please cite this article in press as: Zhang, J., et al., Sedimentology, provenance and geochronology of the Miocene Qiuwu Formation: Implication for the uplift history of Southern Tibet, Geoscience Frontiers (2016), http://dx.doi.org/10.1016/j.gsf.2016.05.010

cluster around 20 Ma, 45–55 Ma, and 80–95 Ma (60%), with peaks at about 46 and 82 Ma. Some zircons show very old ages (22%), between 820 and 3000 Ma (Fig. 9e). The age of the five youngest zircons is 19.4 ± 0.6 Ma, 19.6 ± 0.5 Ma, 20 ± 0.5 Ma, 21 ± 0.5 Ma and 23.4 ± 0.4 Ma, which makes the weighted mean age of 21.0 ± 2.2 Ma (Fig. 9h, Supplementary Table S1). Zircon ages from the top of the section (QW12-40U1) are similar to those from the bottom, but without young cluster around 20 Ma. The major clusters are around 45–60 Ma, 80–100 Ma, and 120–145 Ma (68.7%), with peaks at about 47 and 89 Ma. A few zircons (15%) also yield very old ages, between 830 and 2300 Ma (Fig. 9d).

6. Discussion

6.1. Depositional age of the Qiuwu Formation

Depositional age of the Qiuwu Formation has been controversial. Guo (1975) and Wu (1979) proposed a late Cretaceous deposition based on plant fossil evidences, while subsequent studies suggested late Cretaceous to Eocene (Geng and Tao, 1982) and Eocene (Tao, 1988). Qian (1985) collected more fossils and conducted comparative studies with adjacent formations, whose results indicated a late Paleocene to middle Eocene origin of the Qiuwu Formation. Paleontological evidences had been scarce until Li et al. (2008) applied spore and pollen analyses in attempts of pinpointing the age. The results suggested that Qiuwu Formation was possibly formed during Eocene–Oligocene or even Miocene.

Apart from fossils, the age of the Qiuwu Formation can be restricted by the youngest detrital zircon ages. Dickinson and Gehrels (2009) proposed five measures of the youngest age of a sample using Isoplot: (1) the age of the youngest single grain, YSG; (2) the peak age of the youngest distinct age group, YPP; (3) weighted mean age of the youngest cluster of two or more grain ages overlapping in age at 1σ, YC1σ(2+); (4) weighted mean age of the youngest cluster of three or more grain ages overlapping in age at 2σ, YC2σ(3+); (5) age calculated by the "Youngest Detrital Zircon" routine of Isoplot, YDZ. Here, we use the weighted mean age of 5 grain ages of the youngest cluster (YC) overlapping at 1σ, 21.0 ± 2.2 Ma (Fig. 9h), to constrain the maximum depositional age of the Qiuwu Formation. Considering the discrepancies among different measures for gauging the youngest possible detrital zircon age, the reasonable constraint on the maximum depositional age of the Qiuwu Formation was 19–21 Ma, which falls in early Miocene. The result is consistent with the youngest zircon age 22.5 ± 0.5 Ma in the Qiabulin (Fig. 9a) section obtained by Wang et al. (2013), but is slightly younger than the U–Pb zircon ages derived from the tuff samples (24–26 Ma) of Kailas Formation in the Mount Kailas area (Fig. 9b; DeCelles et al., 2011). Nonetheless, all the detrital zircon ages of the Qiuwu and Kailas formations, both in this and previous studies, show the similar spectra (Fig. 9a–e and references therein).

Table 3
Statistic table of sandstone detrital grains in the Qiuwu Formation.

Sample	Qm	Qp	P	K	Ls	Lm	Lv
QW12–05b2	80	8	83	8	2	8	130
QW12–06b2	67	6	186	3	2	3	49
QW12–07b1	73	12	88	23	2	9	104
QW12–10b1	98	12	70	3	21	42	68
QW12–14b1	89	8	74	17	2	5	106
QW12–19b1	107	4	80	15	6	24	89
QW12–21b1	122	15	18	11	3	6	140
QW12–22b1	52	29	121	19	4	13	65
QW12–22b2	69	36	105	21	1	5	72
QW12–22b4	37	40	150	44	2	7	21
QW12–25b1	14	3	143	94	6	60	20
QW12–25b2	16	29	115	94	3	8	55
QW12–25b3	130	6	106	2	6	65	13
QW12–27b1	116	32	83	12	6	17	62
QW12–27b2	128	10	92	43	7	12	31
QW12–28b1	121	5	83	9	1	10	55
QW12–29b1	142	5	100	8	7	16	45
QW12–31b1	134	19	14	12	8	23	138
QW12–31b3	151	11	7	4	4	11	135
QW12–31b4	200	10	19	4	2	41	56
QW12–32b1	215	15	23	7	5	42	3
QW12–33b1	254	10	12	6	3	22	5

6.2. Provenance of the Qiuwu Formation

Large amount of volcanic detritus occur in the sandstones in the lower part, which plot the sandstones into the transitional arc and dissected arc on the QFL triangular diagram (Fig. 8a). Combined with the southward paleocurrent direction (Fig. 5), the results indicate that the provenance of these sandstones was probably the Gangdese arc in the north. The conclusion is also consistent with the detrital zircon U–Pb ages (Fig. 9e, f and references therein). Intense geochronological studies conducted in the Gangdese arc have revealed that the Gangdese arc has several pulses of magmatic activities since late Triassic (Xie et al., 2011; Guan et al., 2012; Jiang et al., 2012; Ma et al., 2013; Ding et al., 2014; Ji et al., 2014). The Linzizong Group, located on top of the Gangdese arc, is the youngest volcanic rock. Zhu et al. (2015) recently reported precise durations of Linzizong volcanic rocks: 60.2–58.3 Ma for Dianzhong Formation, 55.4–52.6 Ma for Nianbo Formation, and 52.6–52.3 Ma for Pana Formation. Here, we compared the zircon U–Pb ages of Qiuwu Formation with those of Gangdese magmatic rocks (Fig. 9f), and noticed the zircon ages of Gangdese arc show remarkable consistency with the peak value of the Qiuwu Formation.

On the QFL ternary diagram, the plots of the upper part of the section were concentrated in recycled orogen and magmatic arc provenances. In addition, a number of cherts and mafic gravels were observed in the field, which had two possible sources: accretionary wedge and forearc basin in the south, and the Bangong–Nujiang suture in the north of Gangdese. However, the Qiuwu Formation was formed with proximal sediments with low compositional and textural maturity, even though the maturity and stability slightly increased at the later stage. Besides, the Gangdese had already uplifted (Chu et al., 2006; Wen et al., 2008; Ji et al., 2009; Zhu et al., 2011) by the time Qiuwu Formation was formed, blocking the material from the north. Along with the development of Southern Tibet Detachment System (STDS) and Great Central Thrust (GCT) (Yin, 2006), cherts and mafic gravels only had one source from the south, either the ophiolites or forearc basin. Although the detrital zircon spectrum of sample QW12-40U1 from the upper part (Fig. 9d) indicated an ophiolite origin of the sediments, we could not exclude the possibility of a forearc basin source, because of the fact that plenty of basic substances were deposited in forearc area (Einsele et al., 1994; Dürr, 1996; Wu et al., 2010; Wang et al., 2012; An et al., 2014).

Since cherts and mafic gravels did not appear until the very upper part of the section, the most likely explanation would be that the provenance changed during deposition, which suggests that the Yarlung–Zangbo accretionary wedge was high in altitude then. The sandstone petrology (Fig. 8) indicates that the Gangdese arc transited from transitional arc to dissected arc at this time. As a conclusion, the provenances are mainly magmatic arc, subduction-accretionary belt, and fold and thrust belt.

Please cite this article in press as: Zhang, J., et al., Sedimentology, provenance and geochronology of the Miocene Qiuwu Formation: Implication for the uplift history of Southern Tibet, Geoscience Frontiers (2016), http://dx.doi.org/10.1016/j.gsf.2016.05.010

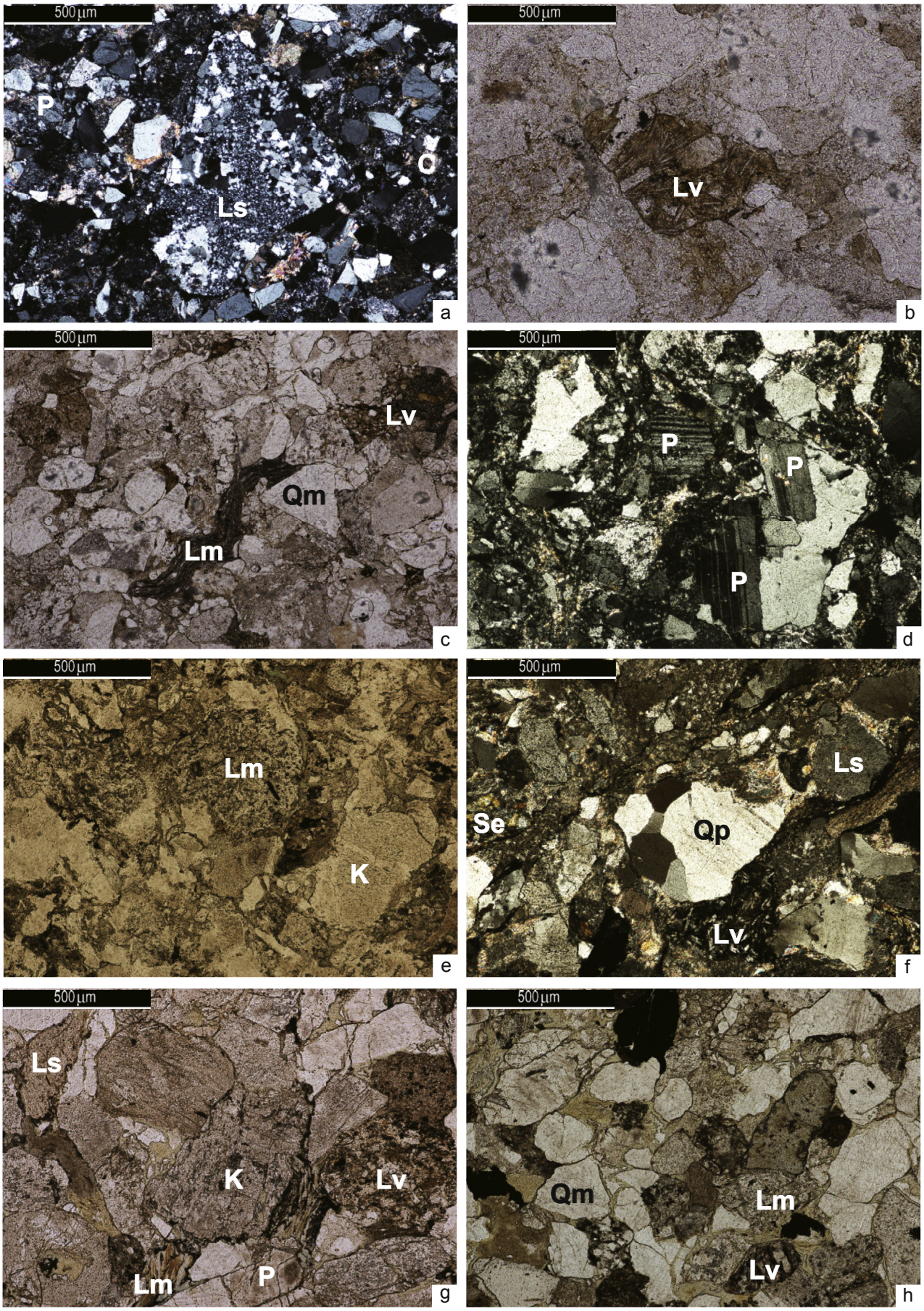

Figure 7. Photographs of thin sections under microscopes. C = calcite; K = potassium feldspar; Lm = metamorphic lithic fragments; Ls = sedimentary lithic fragments; Lv = volcanic lithic fragments; P = plagioclase; Qm = monocrystalline quartz; Qp = polycrystalline quartz; Se = sericite.

Please cite this article in press as: Zhang, J., et al., Sedimentology, provenance and geochronology of the Miocene Qiuwu Formation: Implication for the uplift history of Southern Tibet, Geoscience Frontiers (2016), http://dx.doi.org/10.1016/j.gsf.2016.05.010

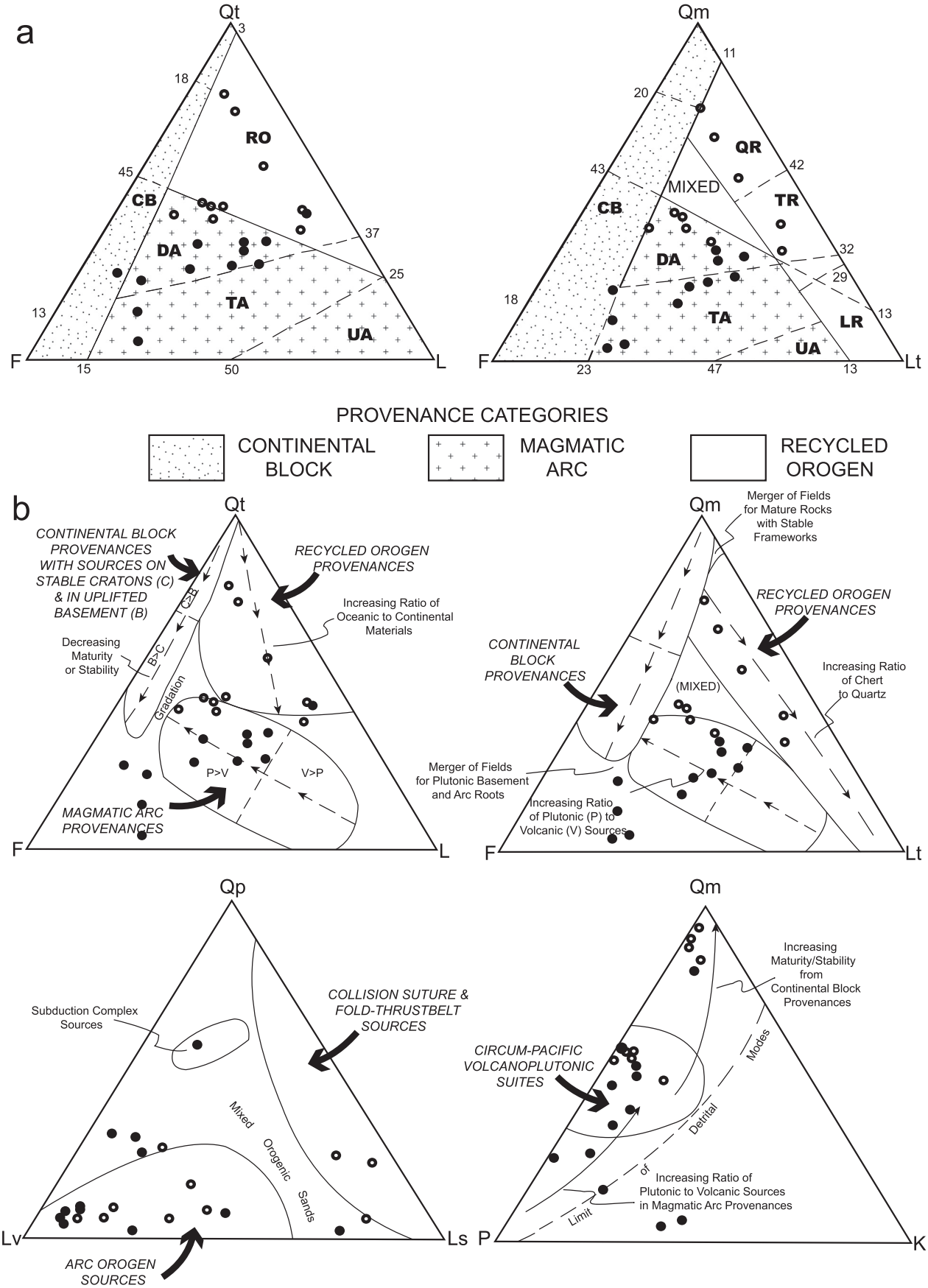

Figure 8. Triplots of sandstone framework compositions. Solid circles represent the lower part, and empty circles represent the upper part. (a) Provisional compositional fields indicative of provenances; (b) actual reported distribution of detrital modes for sandstone from different types of provenances. Qm = monocrystalline quartz; Qp = polycrystalline quartzose lithic fragments; Qt = the total quartzose fragments; P = plagioclase; K = potassium feldspar; F=P + K; Ls = sedimentary lithic fragments; Lv = volcanic lithic fragments; Lt = the total lithic fragments. Provenance field: CB = continental block provenance; RO = recycled orogen provenance; QR = quartzose recycled provenance; TR = transitional recycled provenance; LR = lithic recycled provenance; DA = dissected arc provenance; TA = transitional arc provenance; UA = undissected arc provenance (Dickinson, 1985).

Please cite this article in press as: Zhang, J., et al., Sedimentology, provenance and geochronology of the Miocene Qiuwu Formation: Implication for the uplift history of Southern Tibet, Geoscience Frontiers (2016), http://dx.doi.org/10.1016/j.gsf.2016.05.010

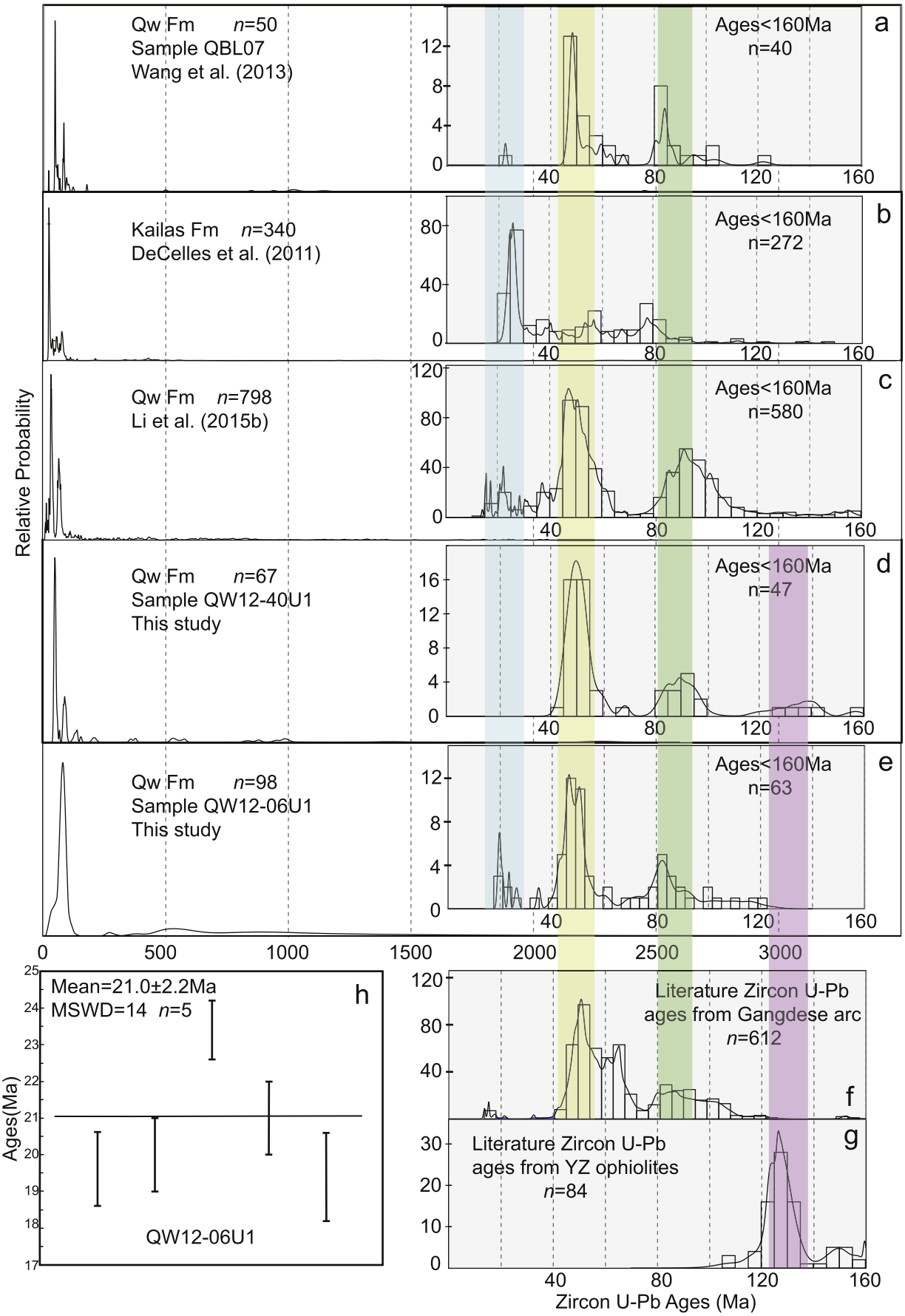

Please cite this article in press as: Zhang, J., et al., Sedimentology, provenance and geochronology of the Miocene Qiuwu Formation: Implication for the uplift history of Southern Tibet, Geoscience Frontiers (2016), http://dx.doi.org/10.1016/j.gsf.2016.05.010

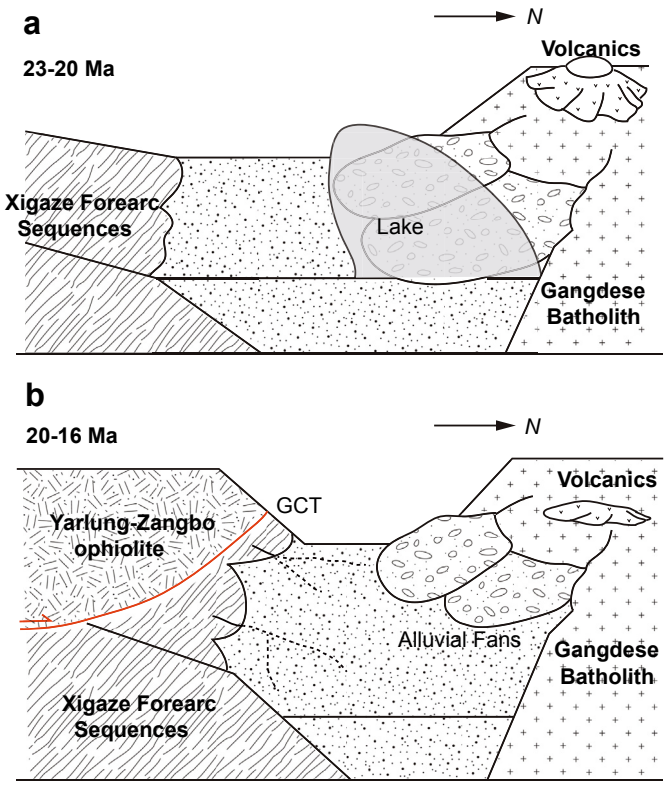

Figure 10. Schematic paleogeographic maps showing the late Oligocene to early Miocene depositional evolution of Qiuwu region. GCT = Great Counter Thrust. See the text for details.

6.3. Depositional mode of the Qiuwu Formation

Based on depositional modes previously proposed for the Kailas Conglomerate (Yin et al., 1999; DeCelles et al., 2011; Wang et al., 2013), the formation of the Qiuwu Formation was associated with continental molasse developing in response to the subsequent India–Asia collision and the development of Great Central Thrust (GCT) (Yin, 2006). Therefore, the development of the section can be divided into two phases (Fig. 10).

Lake and subaqueous fan sediments were deposited along the southern edge of the Gangdese arc at the earlier phase (~23 Ma; Fig. 10a). Tectonic extension, and the subsequent rapid subsidence, possibly resulted from southward rollback of the subducted Indian slab or oblique slip along the suture zone, were the main reasons for the emergence of a series of lakes along the southern margin of the Gangdese arc (DeCelles et al., 2011). In this period, sediments were mainly derived from the Gangdese arc to the north, which is confirmed by paleocurrent data (Fig. 5), and the Yarlung–Zangbo accretionary wedge was still at low elevation. The lakes disappeared at the later phase (ca. 20 Ma; Fig. 10b). A possible reason for the disappearance of lakes is tectonic uplift. According to palynology evidences, the bulk of the Qiuwu Formation was deposited under warm and humid climate (Li et al., 2008). Rapid uplift and erosion of the Himalayan Orogen and the Yarlung–Zangbo suture occurred at this phase (Harrison et al., 1992; White et al., 2002). During the later phase, the development of Great Central Thrust (GCT) accelerated the transportation of detritus from accretionary wedge or forearc basin to piedmont of Gangdese arc. At the same time, the unroofing of the Gangdese arc provided sediments to the Qiuwu Formation. Wang et al. (2013) suggested that the detritus of Qiuwu Formation was entirely from the Gangdese arc, due to the absence of southern source, which contradicts to the change of gravel composition and model sandstone petrology results in our study.

Previous studies suggested the existence of an antecedent Yarlung–Zangbo River (Wang et al., 2013; Carrapa et al., 2014; Li et al., 2015b). However, no sufficient paleocurrent evidence supports this opinion in both the study of Li et al. (2015b) and ours (Fig. 5). The argument that the then newly formed paleo-Yarlung–Zangbo River produced many westward-flowing tributaries (Li et al., 2015b) is untenable due to the lack of westward paleocurrent data in their interpretation. Only one set of data in our study (Fig. 5) supports the possible existence of westward–flowing stage of the paleo-Yarlung–Zangbo River, which could be the result of occasionality and therefore unconvincing. In addition, the relationship between drainage area (A) and river length (L) in modern rivers ($L = aA^b$, the parameters a and b may be of little difference when adopted by different researchers; Hack, 1957; Castelltort et al., 2009) could also be applied to calculating the length of the paleoriver in question. Given that the width of the drainage area is 100 km (an estimation from the inferred provenance) and the length is over 1300 km (DeCelles et al., 2011), the axial river should be no more than 800 m long. However, the paleo-Yarlung–Zangbo River should be longer than 2 km, considering it flowed further to the east into either Red or Irrawaddy Rivers (Clark et al., 2004). In summary, the axial river in the drainage area was not a paleo-Yarlung–Zangbo River, at least, not a drainage system as large as today. More research is required to further verify the existence of the paleo-Yarlung–Zangbo River.

7. Conclusions

Sedimentary and provenance work of the Qiuwu Formation, carried out in this study lead to the following conclusions:

(1) The Qiuwu Formation was a set of terrigenous clastic sediments composed of sandstone, mudstone and conglomerate of different thickness with sedimentary facies changing from subaqueous fans to alluvial fans.
(2) The provenance of the Qiuwu Formation shifted from a single northern source to double sources from both the north and the south.
(3) The Qiuwu Formation was deposited in early Miocene with the weighted mean age of five youngest zircons 21.0 ± 2.2 Ma.
(4) The paleo-Yarlung–Zangbo River may not exist during the development of the Qiuwu Formation.

Figure 9. Relative U–Pb age probability diagrams of detrital zircons from sandstones of the Qiuwu and Kailas formations (a–e), from Gangdese arc (f), and from the Yarlung-Zangbo ophiolites (g), and zircon U–Pb weighted average youngest ages of Qiuwu Formation (h). MSWD = mean square of weighted deviates. Letter '*n*' indicates number of grains in each population. Data of Sample QBL07 of Qiuwu Formation (a) is from Wang et al. (2013). Data of Kailas Formation (b) is after DeCelles et al. (2011). Data of Qiuwu Formation (c) from Li et al. (2015b) contains nine sandstone samples. See detailed data in Supplementary Table S1 for this study (d and e). Also shown for reference are data from the Gangdese magmatic rocks (f; Chu et al., 2006; Wen et al., 2008; Ji et al., 2009; Liang et al., 2010; Xie et al., 2011), and from the Yarlung–Zangbo ophiolites (g; McDermid et al., 2002; Malpas et al., 2003; Wang et al., 2006; Dai et al., 2012; Chan et al., 2015).

Please cite this article in press as: Zhang, J., et al., Sedimentology, provenance and geochronology of the Miocene Qiuwu Formation: Implication for the uplift history of Southern Tibet, Geoscience Frontiers (2016), http://dx.doi.org/10.1016/j.gsf.2016.05.010

Acknowledgments

The 111 Project of China (Grant No. B07011) and the Geological Survey project (No. 1212011221072) provide funding for this research. This is CUGB petro-geochemical contribution No. PGC-201511. We thank Dr. Xi Chen for the help in laboratory and field work. We are very grateful to Dr. Bing Wu at State Key Laboratory of Mineral Deposits Research, Nanjing University, Jiangsu Province, China.

Appendix A. Supplementary data

Supplementary data related to this article can be found at http://dx.doi.org/10.1016/j.gsf.2016.05.010.

References

Aitchison, J.C., Davis, A.M., Badengzhu, Luo, H., 2002. New constraints on the India-Asia collision: the lower Miocene Gangrinboche Conglomerates, Yarlung Tsangpo Suture Zone, SE Tibet. Journal of Asian Earth Sciences 21, 251–263.

Aitchison, J.C., Ali, J.R., Davis, A.M., 2007. When and where did India and Asia collide. Journal of Geophysical Research: Solid Earth (1978–2012) 112, B05423. http://dx.doi.org/10.1029/2006JB004706.

Aitchison, J.C., Xia, X., Baxter, A.T., Ali, J.R., 2011. Detrital zircon U–Pb ages along the Yarlung-Tsangpo suture zone, Tibet: implications for oblique convergence and collision between India and Asia. Gondwana Research 20, 691–709.

Allmendinger, R.W., Cardozo, N., Fisher, D., 2012. Structural geology algorithms: Vectors and tensors in structural geology. Cambridge University Press, Cambridge, 289 pp.

An, W., Hu, X., Garzanti, E., BouDagher-Fadel, M.K., Wang, J., Sun, G., 2014. Xigaze forearc basin revisited (South Tibet): provenance changes and origin of the Xigaze Ophiolite. Geological Society of America Bulletin 126, 1595–1613.

Andersen, T., 2002. Correction of common lead in U-Pb analyses that do not report ^{204}Pb. Chemical Geology 192, 59–79.

Badengzhu, 1979. Xizang Autonomous Region Zhanang-Sangri Regional Geology Reconnaissance Map 1: 50,000. Xizang Geological Survey Geological Team # 2, Group 2, Lhasa.

Badengzhu, 1981. Xizang Autonomous Region Sangri-Jiacha Regional Geology Reconnaissance Map 1: 50,000. Xizang Geological Survey Geological Team # 2, Lhasa.

Black, L.P., Gulson, B.L., 1978. The age of the mud tank carbonatite, strangways range, northern territory. BMR Journal of Australian Geology and Geophysics 3, 227–232.

Blair, T.C., McPherson, J.G., 1994. Alluvial fans and their natural distinction from rivers based on morphology, hydraulic processes, sedimentary processes, and facies assemblages. Journal of Sedimentary Research 64, 450–489.

Carrapa, B., Orme, D.A., DeCelles, P.G., Kapp, P., Cosca, M.A., Waldrip, R., 2014. Miocene burial and exhumation of the India-Asia collision zone in southern Tibet: response to slab dynamics and erosion. Geology 42, 443–446.

Castelltort, S., Simpson, G., Darrioulat, A., 2009. Slope–control on the aspect ratio of river basins. Terra Nova 21, 265–270.

Chan, G.H.N., Aitchison, J.C., Crowley, Q.G., Horstwood, M.S.A., Searle, M.P., Parrish, R.R., Chan, J.S., 2015. U–Pb zircon ages for Yarlung Tsangpo suture zone ophiolites, southwestern Tibet and their tectonic implications. Gondwana Research 27, 719–732.

Chu, M.F., Chung, S.L., Song, B., Liu, D., O'Reilly, S.Y., Pearson, N.J., Ji, J., Wen, D.J., 2006. Zircon U–Pb and Hf isotope constraints on the Mesozoic tectonics and crustal evolution of southern Tibet. Geology 34, 745–748.

Chu, M.F., Chung, S.L., O'Reilly, S.Y., Pearson, N.J., Wu, F.Y., Li, X.H., Liu, D., Ji, J.Q., Chu, C.H., Lee, H.Y., 2011. India's hidden inputs to Tibetan orogeny revealed by Hf isotopes of Transhimalayan zircons and host rocks. Earth and Planetary Science Letters 307, 479–486.

Chu, S., Li, S., 2007. A comparison between two statistic methods about detrital composition of sandstones. Journal of Hefei University of Technology (Natural Science) 3, 668–671 (in Chinese with English abstract).

Clark, M.K., Schoenbohm, L.M., Royden, L.H., Whipple, K.X., Burchfiel, B.C., Zhang, X., Tang, W., Wang, E., Chen, L., 2004. Surface uplift, tectonics, and erosion of eastern Tibet from large-scale drainage patterns. Tectonics 23, TC1006.

Dai, J., Wang, C., Hébert, R., Li, Y., Zhong, H., Guillaume, R., Bezard, R., Wei, Y., 2011. Late Devonian OIB alkaline gabbro in the Yarlung Zangbo suture zone: remnants of the Paleo-Tethys? Gondwana Research 19, 232–243.

Dai, J., Wang, C., Li, Y., 2012. Relicts of the early cretaceous seamounts in the central-western Yarlung Zangbo Suture Zone, southern Tibet. Journal of Asian Earth Sciences 53, 25–37.

Dai, J., Wang, C., Hourigan, J., Li, Z., Zhuang, G., 2013a. Exhumation history of the Gangdese batholith, southern Tibetan Plateau: evidence from apatite and zircon (U-Th)/He thermochronology. The Journal of Geology 121, 155–172.

Dai, J., Wang, C., Polat, A., Santosh, M., Li, Y., Ge, Y., 2013b. Rapid forearc spreading between 130 and 120Ma: evidence from geochronology and geochemistry of the Xigaze ophiolite, southern Tibet. Lithos 172, 1–16.

Davis, A.M., Aitchison, J.C., Badengzhu, Luo, H., Zyabrev, S., 2002. Paleogene island arc collision-related conglomerates, Yarlung Tsangpo suture zone, Tibet. Sedimentary Geology 150, 247–273.

DeCelles, P.G., Kapp, P., Quade, J., Gehrels, G.E., 2011. Oligocene-Miocene Kailas basin, southwestern Tibet: record of postcollisional upper-plate extension in the Indus-Yarlung suture zone. Geological Society of America Bulletin 123, 1337–1362.

Dickinson, W.R., 1985. Interpreting provenance relations from detrital modes of Sandstones. Provenance of Arenites 148, 333–361.

Dickinson, W.R., Suczek, C.A., 1979. Plate petonics and sandstone compositions. The American Association of Petroleum Geologists Bulletin 63, 2164–2182.

Dickinson, W.R., Gehrels, G.E., 2009. Use of U-Pb ages of detrital zircons to infer maximum depositional ages of strata: a test against a Colorado Plateau Mesozoic database. Earth and Planetary Science Letters 288, 115–125.

Ding, L., Kapp, P., Wan, X., 2005. Paleocene-Eocene Record of Ophiolite Obduction and Initial India-Asia Collision, South Central Tibet. Tectonics 24.

Ding, L., Xu, Q., Yue, Y., Wang, H., Cai, F., Li, S., 2014. The Andean-type Gangdese mountains: Paleoelevation record from the Paleocene–Eocene Linzhou basin. Earth and Planetary Science Letters 392, 250–264.

Dürr, S.B., 1996. Provenance of Xigaze fore-arc basin clastic rocks (Cretaceous, south Tibet). Geological Society of America Bulletin 108, 669–684.

Einsele, G., Liu, B., Dürr, S., Frisch, W., Liu, G., Luterbacher, H.P., Ratschbacher, L., Ricken, W., Wendt, J., Wetzel, A., Yu, G., Zheng, H., 1994. The Xigaze forearc basin: evolution and facies architecture (Cretaceous, Tibet). Sedimentary Geology 90, 1–32.

Gansser, A., 1964. Geology of the Himalayas. Interscience, New York, 289 pp.

Geng, G., Tao, J., 1982. Tertiary plants from Xizang. In: Series of the Scientific Expedition to the Qinghai-Xizang Plateau: Palaeontology of Xizang. Science, Beijing, pp. 110–123 (in Chinese).

Gillet, H., Lericolais, G., Réhault, J.P., 2007. Messinian event in the Black Sea: evidence of a Messinian erosional surface. Marine Geology 244, 142–165.

Griffin, W.L., Belousova, E.A., Shee, S.R., Pearson, N.J., O'Reilly, S.Y., 2004. Archean crustal evolution in the northern Yilgarn Craton: U-Pb and Hf-isotope evidence from detrital zircons. Precambrian Research 131, 231–282.

Guan, Q., Zhu, D.C., Zhao, Z.D., Dong, G.C., Zhang, L.L., Li, X.W., Liu, M., Mo, X.X., Liu, Y.S., Yuan, H.L., 2012. Crustal thickening prior to 38Ma in southern Tibet: evidence from lower crust-derived adakitic magmatism in the Gangdese Batholith. Gondwana Research 21, 88–99.

Guo, S., 1975. The plant fossil of the Xigaze group from Mount Qomolangma region. In: Report of Scientific Expedition to Mt. Jolmo Lungma Region. Science, Beijing, pp. 411–425 (in Chinese).

Hack, J.T., 1957. Studies of longitudinal stream profiles in Virginia and Maryland. U.S. Geological Survey Professional Paper 294-B, 97 pp.

Harrison, T.M., Copeland, P., Kidd, W.S., Yin, A., 1992. Raising Tibet. Science 255, 1663–1670.

Horton, B.K., Schmitt, J.G., 1996. Sedimentology of a lacustrine fan-delta system, Miocene Horse Camp Formation, Nevada, USA. Sedimentology 43, 133–155.

Horton, B.K., Yin, A., Spurlin, M.S., Zhou, J., Wang, J., 2002. Paleocene–Eocene syncontractional sedimentation in narrow, lacustrine-dominated basins of east-central Tibet. Geological Society of America Bulletin 114, 771–786.

Ingersoll, R.V., Bullard, T.F., Ford, R.L., Grimm, J.P., Pickle, J.D., Sares, S.W., 1984. The effect of grain size on detrital modes: a test of the Gazzi-Dickinson point-counting method. Journal of Sedimentary Research 54, 103–116.

Jackson, S.E., Pearson, N.J., Griffin, W.L., Belousova, E.A., 2004. The application of laser ablation-inductively coupled plasma-mass spectrometry to in situ U-Pb zircon geochronology. Chemical Geology 211, 47–69.

Ji, W.Q., Wu, F.Y., Chung, S.L., Li, J.X., Liu, C.Z., 2009. Zircon U–Pb geochronology and Hf isotopic constraints on petrogenesis of the Gangdese batholith, southern Tibet. Chemical Geology 262, 229–245.

Ji, W.Q., Wu, F.Y., Chung, S.L., Li, J.X., Liu, C.Z., 2014. The Gangdese magmatic constraints on a latest Cretaceous lithospheric delamination of the Lhasa terrane, southern Tibet. Lithos 210, 168–180.

Jiang, Z.Q., Wang, Q., Li, Z.X., Wyman, D.A., Tang, G.J., Jia, X.H., Yang, Y.H., 2012. Late Cretaceous (ca. 90Ma) adakitic intrusive rocks in the Kelu area, Gangdese belt (southern Tibet): slab melting and implications for Cu–Au mineralization. Journal of Asian Earth Sciences 53, 67–81.

Li, G., Kohn, B., Sandiford, M., Xu, Z., Wei, L., 2015a. Constraining the age of Liuqu Conglomerate, southern Tibet: implications for evolution of the India–Asia collision zone. Earth and Planetary Science Letters 426, 259–266.

Li, J., David, J.B., Zhang, Y., 2008. Palynological indications of environmental changes during the Late Cretaceous-Eocene on the southern continental margin of Laurasia, Xizang (Tibet). Palaeogeography, Palaeoclimatology, Palaeoecology 265, 78–86.

Li, J., Guo, Z., David, J.B., Cai, H., Zhang, Y., 2010. Palynological stratigraphy of the late cretaceous and Cenozoic collision-related conglomerates at Qiabulin, Xigaze, Xizang (Tibet) and its bearing on palaeoenvironmental development. Journal of Asian Earth Sciences 38, 86–95.

Li, S., Ding, L., Xu, Q., Wang, H., Yue, Y., Baral, U., 2015b. The evolution of Yarlung Tsangpo River: constraints from the age and provenance of the Gangdese Conglomerates, southern Tibet. Gondwana Research. http://dx.doi.org/10.1016/j.gr.2015.05.010.

Liang, Y., Zhu, J., Ci, Q., He, W., Zhang, K., 2010. Zircon U-Pb ages and geochemistry of volcanic rock from Linzizong Group in Zhunuo area in middle Gangdise Belt, Tibet Plateau. Earth Science—Journal of China University of Goesciences 35, 211–223 (in Chinese with English abstract).

Link, M.H., Osborne, R.H., 1978. Lacustrine facies in the Pliocene Ridge Basin Group: Ridge basin, California. In: Matter, A., Tucker, M.E. (Eds.), Modern and Ancient Lake Sediments. International Association of Sedimentologists Special Publication 2, pp. 169–187.

Ludwig, K.R., 2001. User's manual for Isoplot/Ex rev. 2. 49, a geochronological toolkit for Microsoft Excel. Berkeley Geochronology Center Special Publications 1, 1–55.

Ma, L., Wang, Q., Li, Z.X., Wyman, D.A., Jiang, Z.Q., Yang, J.H., Gou, G.N., Guo, H.F., 2013. Early Late Cretaceous (ca. 93Ma) norites and hornblendites in the Milin area, eastern Gangdese: lithosphere–asthenosphere interaction during slab roll-back and an insight into early Late Cretaceous (ca. 100–80Ma) magmatic "flare-up" in southern Lhasa (Tibet). Lithos 172, 17–30.

Malpas, J., Zhou, M.F., Robinson, P.T., Reynolds, P.H., 2003. Geochemical and geochronological constraints on the origin and emplacement of the Yarlung Zangbo ophiolites, Southern Tibet. Geological Society, London, Special Publications 218, 191–206.

McDermid, I.R.C., Aitchison, J.C., Davis, A.M., Harrison, T., Grove, M., 2002. The Zedong terrane: a Late Jurassic intra-oceanic magmatic arc within the Yarlung–Tsangpo suture zone, southeastern Tibet. Chemical Geology 187, 267–277.

Miall, A.D., 1996. The Geology of Fluvial Deposits. Springer, Berlin, 582 pp.

Miall, A.D., 1977. A review of the braided-river depositional environment. Earth Science Reviews 13, 1–62.

Mo, X., Niu, Y., Dong, G., Zhao, Z., Hou, Z., Zhou, S., Ke, S., 2008. Contribution of syncollisional felsic magmatism to continental crust growth: a case study of the Paleogene Linzizong volcanic succession in southern Tibet. Chemical Geology 250, 49–67.

Nemec, W., Postma, G., 1993. Quaternary alluvial fans in southwestern Crete: sedimentation processes and geomorphic evolution. In: Marzo, M., Puigdefábregas, C. (Eds.), Alluvial Sedimentation. International Association of Sedimentologists Special Publication 17, pp. 235–276.

Olivier, N., Dromart, G., Coltice, N., Flament, N., Rey, P., Sauvestre, R., 2012. A deep subaqueous fan depositional model for the Palaeoarchaean (3.46 Ga) Marble Bar Cherts, Warrawoona Group, Western Australia. Geological Magazine 149, 743–749.

Orme, D.A., Carrapa, B., Kapp, P., 2015. Sedimentology, provenance and geochronology of the upper Cretaceous-lower Eocene western Xigaze forearc basin, southern Tibet. Basin Research 27, 387–411.

Pan, G.T., Ding, J., Yao, D.S., Wang, L.Q., 2004. Geological Map of Qinghai-Tibet Plateau and Adjacent Regions. Chengdu Map Publishing, Chengdu.

Pettijohn, F.J., 1957. Sedimentary Rocks. Harper and Brothers, New York, 718 pp.

Qian, D., 1985. A discussion on the age of Qiuwu coal measures and preliminary correlation of the molasses formation at the Ladakh-Gandise marginal mountain chain. In. Contributions to the geology of the Qinghai-Xizang (Tibet) Plateau 16, 229–241 (in Chinese).

Ridgway, K.D., DeCelles, P.G., 1993. Stream-dominated alluvial fan and lacustrine depositional systems in Cenozoic strike-slip basins, Denali fault system, Yukon Territory, Canada. Sedimentology 40, 645–666.

Searle, M.P., Windley, B.F., Coward, M.P., Cooper, D.J.W., Rex, A.J., Li, T., Xiao, X., Jan, M.Q., Thakur, V.C., Kumar, S., 1987. The closing of the Tethys and the tectonics of the Himalaya. Geological Society of America Bulletin 98, 678–701.

Smith, G.A., 1986. Coarse-grained nonmarine volcaniclastic sediment: terminology and depositional process. Geological Society of America Bulletin 97, 1–10.

Tao, J., 1988. Plant fossils from Liuqu Formation in Lhaze County, Xizang and their palaeoclimatological significances. Monograph of Institute of Geology, Chinese Academy of Sciences 3, 223–238 (in Chinese).

Walker, R.G., 1978. Deep-water sandstone facies and ancient submarine fans: models for exploration for stratigraphic traps. American Association of Petroleum Geologists Bulletin 62, 932–966.

Wang, C., Li, X., Hu, X., Jansa, L.F., 2002. Latest marine horizon north of Qomolangma (Mt Everest): implications for closure of Tethys seaway and collision tectonics. Terra Nova 14, 114–120.

Wang, C., Li, X., Liu, Z., Li, Y., Jansa, L., Dai, J., Wei, Y., 2012. Revision of the Cretaceous-Paleogene stratigraphic framework, facies architecture and provenance of the Xigaze forearc basin along the Yarlung Zangbo suture zone. Gondwana Research 22, 415–433.

Wang, J.G., Hu, X.M., Wu, F.Y., Jansa, L., 2010. Provenance of the Liuqu Conglomerate in southern Tibet: a Paleogene erosional record of the Himalayan-Tibetan orogeny. Sedimentary Geology 231, 74–84.

Wang, J.G., Hu, X.M., Garzanti, E., Wu, F.Y., 2013. Upper Oligocene-Lower Miocene Gangrinboche Conglomerate in the Xigaze area, southern Tibet: implications for Himalayan uplift and paleo-Yarlung-Zangbo initiation. The Journal of Geology 121, 425–444.

Wang, R., Xia, B., Zhou, G., Zhang, Y., Yang, Z., Li, W., Wei, D., Zhong, L., Xu, L., 2006. SHRIMP zircon U-Pb dating for gabbro from the Tiding ophiolite in Tibet. Chinese Science Bulletin 51, 1776–1779.

Wei, B.J., Peng, Y.H., 1984. Xizang Autonomous Region Xigaze—Qushui Geological Traverse Map 1:200,000. Xizang Geological Survey Geological Team # 2, Lhasa.

Weirich, F.H., 1988. Field evidence for hydraulic jumps in subaqueous sediment gravity flows. Nature 332, 626–629.

Wen, D.R., Liu, D., Chung, S.L., Chu, M.F., Ji, J., Zhang, Q., Song, B., Lee, T.Y., Yeh, M.W., Lo, C.H., 2008. Zircon SHRIMP U/Pb ages of the Gangdese Batholith and implications for Neotethyan subduction in southern Tibet. Chemical Geology 252, 191–201.

White, N.M., Pringle, M., Garzanti, E., Bickle, M., Najman, Y., Chapman, H., Friend, P., 2002. Constraints on the exhumation and erosion of the High Himalayan Slab, NW India, from foreland basin deposits. Earth and Planetary Science Letters 195, 29–44.

Wu, F.Y., Ji, W.Q., Liu, C.Z., Chung, S.L., 2010. Detrital zircon U-Pb and Hf isotopic data from the Xigaze fore-arc basin: constraints on Transhimalayan magmatic evolution in southern Tibet. Chemical Geology 271, 13–25.

Wu, Y., 1979. The late cretaceous coal series of Xizang. In: Contribution to the geology of the Qinghai Xizang (Tibet) Plateau 3, pp. 212–223 (in Chinese).

Xie, K., Zeng, L., Liu, J., Gao, L., Hu, G., 2011. Timing and geochemistry of the Linzizong Group volcanic rocks in Sangsang area, Ngamring County, southern Tibet. Geological Bulletin of China 30, 1339–1352 (in Chinese with English abstract).

Yin, A., Harrison, T.M., Murphy, M.A., Grove, M., Nie, S., 1999. Tertiary deformation history of southeastern and southwestern Tibet during the Indo-Asian collision. Geological Society of America Bulletin 111, 1644–1664.

Yin, A., Harrison, T.M., 2000. Geologic evolution of the Himalayan-Tibetan orogeny. Annual Review of Earth and Planetary Sciences 28, 211–280.

Yin, A., 2006. Cenozoic tectonic evolution of the Himalayan Orogen as constrained by along-strike variation of structural geometry, exhumation history, and foreland sedimentation. Earth Science Review 76, 1–131.

Yin, J., Sun, X., Sun, Y., Liu, C., 1988. Stratigraphy on the molasse-type sediments of the paired molasse belts in Xigaze area. Monograph of Institute of Geology. Chinese Academy of Sciences 3, 158–176 (in Chinese).

Yu, B., Cantelli, A., Marr, J., Pirmez, C., O'Byrne, C., Parker, G., 2006. Experiments on self-channelized subaqueous fans emplaced by turbidity currents and dilute mudflows. Journal of Sedimentary Research 76, 889–902.

Zhang, S.M., Fu, X.L., 1982. Xizang Autonomous Region Xigaze—Saga Geological Traverse Map 1:200,000. Xizang Geological Survey Geological Team # 2, Lhasa.

Zhu, D.C., Zhao, Z.D., Niu, Y., Mo, X.X., Chung, S.L., Hou, Z.Q., Wang, L.Q., Wu, F.Y., 2011. The Lhasa terrane: record of a microcontinent and its histories of drift and growth. Earth and Planetary Science Letters 301, 241–255.

Zhu, D.C., Wang, Q., Zhao, Z.D., Chung, S.L., Cawood, P.A., Niu, Y., Liu, S.A., Wu, F.Y., Mo, X.X., 2015. Magmatic Record of India-Asia Collision. Scientific reports 5.

Please cite this article in press as: Zhang, J., et al., Sedimentology, provenance and geochronology of the Miocene Qiuwu Formation: Implication for the uplift history of Southern Tibet, Geoscience Frontiers (2016), http://dx.doi.org/10.1016/j.gsf.2016.05.010